Nat. Hazards Earth Syst. Sci. Discuss., 2, 5575–5601, 2014
www.nat-hazards-earth-syst-sci-discuss.net/2/5575/2014/
doi:10.5194/nhessd-2-5575-2014

Natural Hazards and Earth System Sciences
Open Access
Discussions

Susceptibility assessment of landslides under extreme-rainfall events using hydro-geotechnical model; a case study of Umyeonsan (Mt.), Korea

S. S. Jeong[1], J. H. Kim[1], Y. M. Kim[1], and D. H. Bae[2]

[1]Department of civil engineering, Yonsei university, Seoul, Republic of Korea
[2]Department of Civil Engineering, Sejong university, Seoul, Republic of Korea

Received: 27 June 2014 – Accepted: 13 July 2014 – Published: 28 August 2014

Correspondence to: J. H. Kim (hwanee2@gmail.com)

Published by Copernicus Publications on behalf of the European Geosciences Union.

Abstract

The influence of climate change on patterns has the potential to alter stability of partially saturated soil slopes. Changes in rainfall patterns have a strong influence on stability of partially saturated soil slopes, which recently have resulted in shallow landslides. In this paper, a comprehensive case study on the 2011 Umyeonsan (Mt.) landslides was highlighted. The incident involves the collapse of a soil slope and the debris flow under extreme-rainfall event, causing 16 fatalities and serious damaged to 146 housings. A fundamental study was carried out on the cause and mechanism of landslide/debris flow. An analytical method is developed for determining the failure mechanism of unsaturated soil slopes under extreme-rainfall, the effect of groundwater flow; the downward velocity of wetting front, and the upward velocity of groundwater level. Based on this, we propose the conceptual methodology of landslide design based on experimental tests and numerical analyses which consider the important mechanism of the combined effects of both groundwater flow and rainfall infiltration into the slope.

1 Introduction

Global climate change led to fluctuations in rainfall pattern. In South Korea, the frequency and intensity of heavy rainfall have increased during the summer seasons, and as a result to trigger more landslides, which are characterised by a relatively shallow failure of surfaces that develop parallel to the original slope (Jeong et al., 2008; Kim et al., 2012).

A record heavy rainfall hits the whole land area, Korea on June and July of 2011. Early in the morning of 27 July, about 150 small and large landslides occurred in 13 villages all over Umyeonsan (Mt.) where is located in downtown of Seoul metropolis with the height of 312.6 m a.s.l. Because the mountain is located at the centre of a dense residential area, the hazard had a great impact on the society compared to debris flows that occur in rural areas, and it led to careful scrutiny of the hazard area. Severe

NHESSD
2, 5575–5601, 2014

rainfall-induced landslides with slope failure and debris flow occurred in four villages of Raemian, Shindonga, Jeonwon, and Hyeongchon at Umyeonsan (Mt.). Some of the landslides hit the villages near the lower part of Umyeonsan (Mt.), causing the most casualties. Some landslides evolved from debris flows, flowing into the roads, victimizing the people passing the streets. The landslides rapidly expanded into a fast debris flow spreading throughout the narrow and sloping roads, invading many villages and roads. In many cases the debris flow overflowed into the outer part of Umyeonsan (Mt.).

This paper aims to investigate the cause of the landslides of Umyeonsan (Mt.) 2011, and to propose the conceptual methodology of landslide design based on lab and field tests and numerical analyses which consider the important mechanism of groundwater flow and rainfall infiltration into the slope using a new approach on the source of rainfall-induced landslide.

2 Climate change

A broad consensus that the Earth's surface and oceans are warming at rates unprecedented in the historical record prevails in the scientific community. Global warming will also affect the hydrologic cycle by directly increasing evaporation of available surface water and vegetation transpiration (IPCC, 2007). It is affecting regional weather patterns, rainfall trends, and their variability. These changes potentially have a strong on stability of partially saturated soil slopes. These changes could trigger deformation of the Umyeonsan (Mt.) soil slopes resulting in slope instability within many mountainous areas of South Korea (Jeong et al., 2008). Hence, it is needed to investigate the influence of changes in trend and frequency of rainfall patterns observed through the rainfall data collected over a relatively long period on the stability analysis of partially saturated soil slopes. The quantitative increase and frequency change of recent rainfall patterns often cause shallow soil slope failures in comparison with past rainfall patterns.

In South Korea, global climate change which led to fluctuations in rainfall pattern like sub-tropical regions. Figure 1 shows 4 sites among 56 sites where continuous

NHESSD
2, 5575–5601, 2014

daily data are collected for peak rainfalls over 33 year period. Geochang, Yeongju, Inje, and Jecheon areas are the 4 selected mountainous sites in South Korea as indicated by circles in the right of Fig. 1a. Figure 1b demonstrate an increasing trend in rainfall intensity for these 4 sites. The results show annual daily maximum (in mm) for the whole observation period from 1973 to 2006. The plots illustrate that steadily increasing trend in rainfall intensity was observed throughout the 33 year period.

According to report from Korean Meteorological Administration (KMA), the seasonal intense rainfall on the study area, the Umyeonsan (Mt.), prolonged for two months (1105 mm), and 304 mm of heavy rain fell the last one day (KMA, 2011). It reported that the cumulative rainfall for 2 months before landslides event in 2011 was unprecedented in the last 10 years.

3 Umyeonsan (Mt.) slope hazard sites

Umyeonsan (Mt.) lies at 37°28′2″ N latitude and 127°0′25″ E longitude with a height of 312.6 m. It has a main ridge formed from the northeast to the southwest, including six valleys perpendicular to the main ridge. Most of the mountain consists of lacustrine biotite gneiss. Two typhoons, i.e. Typhoon Meari (22–27 June) and Typhoon Muifa (28 July to 9 August) occurred in 2011, and the seasonal rain front remained in the middle of the Korean peninsula including the Umyeonsan (Mt.). They produced much more rainfall compared to the average rainfall and eventually led to landslides and debris flows around the Umyeonsan (Mt.).

A large amount of data, such as longitude/latitude and topographical/geotechnical characteristics in places where landslides had occurred, was collected by field surveys using a portable GPS, a laser ranger and a clinometer. Based on this, the coordinates regarding landslides were indicated on an aerial photograph of the area around Mt. Umyeonsan, as shown in Fig. 2a. The landslide locations are marked by coloured dots, and the debris flow routes are marked by sky-blue lines. Most of the debris flows resulted from landslides and flowed downward to the stream. They occurred

NHESSD
2, 5575–5601, 2014

simultaneously over the whole Umyeonsan (Mt.) area. Among these, two test sites were selected for landslide analysis in this study. The sites are the Raemian watershed (test site 1) and the Dukwooam watershed (test site 2) shown in Fig. 2b. The surface areas of the two watersheds are 128 700 and 98 700 m^2, respectively. Under heavy rainfall, in test sites 1 and 2, 6 and 4 landslides (46 and 44 landslides per km^2 with an average of 34 landslides km^2) were generated with 685 and 49 m^2 (0.53 and 0.05 % with an average of 0.04 %), respectively.

4 Umyeonsan (Mt.) slope hazard sites

The better way for identifying the sloping to soil behaviour is to collect the material properties of unsaturated soils through the laboratory and field tests. That is why a matric suction that reflects rainfall infiltration into soils is very important to analyse rainfall-induced landslides. Therefore, the volumetric water content is estimated as a function of the matric suction of soil by laboratory test and the initial matric suction is measured in the field.

4.1 The mathematics of development

The SWCC is can be used to derive permeability functions for use in unsaturated groundwater flow problems and to establish unsaturated shear strength parameters (Vanapalli et al., 1996). To obtain the SWCC of top soil on the Raemian watershed of Umyeonsan (Mt.), Geotechnical Consulting and Testing Systems (GCTS) pressure plate extractor (Pham and Fredlund, 2004) and filter paper test were performed. The GCTS pressure plate consists of two main parts which comprise a pressure chamber and a loading system. The pressure chamber can be subjected to extremely high air pressure (i.e. from 0.1 to 1500 kPa). Filter paper test as specified in ASTM D5298-10 (ASTM, 2012) was used for defining the SWCC for the condition of high matric suction

NHESSD
2, 5575–5601, 2014

(more than 1000 kPa of matric suction). The filter paper of Whatman No. 42 was used (Kim et al., 2004).

The results of these tests are given in Table 1. According to the Unified Soil Classification System (USCS), the top soil can be classified as SM (silty sand). It is found that the tests done by GTCS pressure plate extractor showed a higher air-entry value, saturated- and residual volumetric water content. From this SWCC tests, the volumetric water-contents corresponding to matric suction by field measurement were adopted for calculating wetting band depth, infiltration depth and recharge depth in this study.

4.2 The chemistry of development

The values for the matric suction were measured at test site 1 from 29 June to the 19 July 2012. Three tensiometers depending on shallow- and middle- and deep-depths were installed and then measured matric suctions at the total of six different locations (T1–T6), as shown in Fig. 3a. Typically monitored results at T2 and T5 have been selected and are shown in Fig. 3b and c. The initial matric suction measured at the site on 29 June before the rainy season was approximately 75–85 kPa. After the rainfall began the matric suctions of 0.2–0.6 m depths rapidly decreased to 0–16 kPa and the matric suctions of 0.6–1.3 m gradually decreased to 20 kPa. For the depth of 1.4 m, the matric suction did not change during the six days, since the infiltrated rainwater did not reach to this depth, whereas, it tends to decrease after the 6th day. Since then, all tensiometers were maintained approximately at 10–20 kPa without further additional rainfall. Therefore, in the landslide analysis, the matric suctions of 80 and 20 kPa were adopted as an initial matric suctions for dry- and unsaturated soils, respectively.

5 Proposed methodology: YS-slope model

The proposed model (referred to as YS-slope model) is to simulate the potential occurrences of shallow landslides on unsaturated soil by rainfall-infiltration, storage,

NHESSD
2, 5575–5601, 2014

recharge and groundwater flow processes. This physically-based prediction model was based on geographic information system (GIS) (Soller et al., 1999, 2005), all of data sets, topographic, soil depth, precipitation and geotechnical parameters were built to raster data of matrix structure.

5.1 Geotechnical model

Landslide analysis considers the infiltration by rainfall, which can be classified into three mechanisms: (1) a mechanism that considers the downward velocity of the wetting front, (2) a mechanism that considers the upward velocity of the groundwater level, and (3) a mechanism that considers both of these factors. YS-Slope model improves infinite slope model for the first or second case to interpret the landslide susceptibility for the third of the mechanisms.

The Mohr–Coulomb criteria for simulating the unsaturated soil strength that was adopted in the stability analysis has been improved by considering the pore water pressure and pore-air pressure (Pradel and Raad, 1993). The uniform load from the vegetation and constant number of additional shear strengths from the roots of vegetation are considered as described by Hammond (Hammond et al., 1992). As shown in Fig. 4a, the safety factor (FS) for the infinite slope is calculated from the ratio of the resisting stress on a slip surface to the gravitationally induced downward slope driving stress:

$$\mathrm{FS} = \frac{(c'_{\mathrm{s}} + c'_{\mathrm{r}}) + \{(\gamma_{\mathrm{sat}} \cdot D_{\mathrm{w}} + q_0) - (\gamma_{\mathrm{w}} \cdot D_{\mathrm{w}})\} \cos^2\beta \cdot \tan\phi'}{(\gamma_{\mathrm{sat}} \cdot D_{\mathrm{w}} + q_0) \cdot \sin\beta \cdot \cos\beta} \quad (1)$$

where c'_{s} is the cohesion of the soil, c'_{r} is the constant value related to additional shear strengths from the roots of trees, q_0 is the uniform load by trees, D_{w} is the depth of the wetting band ($= D_{\mathrm{wm}} + D_{\mathrm{wn}}$), D_{s} is the depth of the unsaturated soil ($= D_{\mathrm{mn}}$), γ_{t} is the total unit weight of the soil, γ_{sat} is the saturated unit weight of the soil, γ_{w} is the unit weight of water, and β is the angle of the slope.

NHESSD
2, 5575–5601, 2014

5.2 Hydrological model

The hydrologic model has been improved by incorporating the combined effects of groundwater flow and rainfall infiltration to the raster model (Soller et al., 1999; Smit, 2000). This model was developed by considering the unsaturated soil behaviour to estimate the rainfall-infiltration (I_R) and the recharge (R). The basic assumptions applied to the hydrologic model are that the aquifer is homogeneous, the recharge is non-uniform and varies over time, and the groundwater flows only below the groundwater table.

The soil profile is ideally subdivided into three zones, i.e. the wetting band zone, partially saturated zone, and fully saturated zone, as shown in Fig. 4b. The vertical infiltration of water from the surface into the ground is modelled in the wetting band and partially saturated zones, and the storage time is also considered. The storage time is defined as elapsed time at which rainwater infiltrates into the groundwater through the unsaturated zone. The horizontal movement of the groundwater is generated when the infiltrated water recharges into the fully saturated zone (Table 2).

5.3 Rainfall-infiltration model

Commonly used Green-Ampt model (Green and Ampt, 1911) for one-dimensional rainfall-infiltration was modified and used to calculate infiltration depth and recharge depth. The proposed model assumed that the volumetric water content and deficit the water content remain constant above or below the wetting front, as shown in Fig. 4b. The rainfall infiltration (I_R) could be represented as Eq. (2), and it is estimated by the trial and error method with a variable of cumulative infiltration. The ponding time (Eq. 3) was considered to estimate the relationship between the rainfall-infiltration and runoff (Mein and Larson, 1973). The depth of the wetting front (D_{wn}) in the vadose zone is defined as the ratio of the rainfall-infiltration (I_R) and the deficit water content ($\Delta\theta$) in Eq. (4):

NHESSD
2, 5575–5601, 2014

$$I_R = I \cdot t_p + \int_{t_p}^{t_w} K_s \left(1 + \frac{\psi_f \cdot \Delta\theta}{F}\right) \quad (2)$$

$$t_p = \frac{K_s \cdot \psi_f \cdot \Delta\theta}{I_R \cdot (K_s - I_R)} \quad (3)$$

$$D_{wn} = \frac{I_R}{\Delta\theta} = \frac{I \cdot t_p + \int_{t_p}^{t_w} K_s \left(1 + \frac{\psi_f \cdot \Delta\theta}{F}\right)}{\Delta\theta} \quad (4)$$

where I is the rainfall intensity, t_p is the time for ponding, t_w is the rainfall duration, K_s is the saturated permeability, ψ_f is the head of metric suction, F is the cumulative infiltration depth and $\Delta\theta$ is the deficit water content.

5.4 Groundwater flow model

The groundwater flow was derived for a small elemental volume, for which the properties of the soil were assumed to be effectively constant. A mass balance was done on the water flowing in and out of this small volume, and the flux was calculated in terms of the head using constitutive equation of Darcy's law (Eq. 5), which requires that the flow is slow (Fig. 5). Therefore, a form of the Laplace equation describes this steady-state flow of the groundwater as following Eq. (14). The kinetic energy is neglected as described by Cedergren (1977).

$$v = ki = k\frac{dh}{ds} \quad (5)$$

$$\frac{\partial}{\partial x}\left(k_x \frac{\partial h}{\partial x}\right) + \frac{\partial}{\partial y}\left(k_y \frac{\partial h}{\partial y}\right) + \frac{\partial}{\partial z}\left(k_z \frac{\partial h}{\partial z}\right) = 0 \quad (6)$$

where v is the seepage velocity, k is the permeability, i is hydraulic gradient, s is the distance through the soil, and the subscript x (or y, z) denotes the x (or y, z) direction.

NHESSD
2, 5575–5601, 2014

The variable h is the groundwater potential, equal to the sum of the kinetic energy, pressure and potential energy heads as in (Eq. 7):

$$h = \frac{v^2}{2g} + \frac{p}{\rho g} + z \approx \frac{p}{\rho g} + z \tag{7}$$

The total volume of the flow leaving the element (Q_x) in the x direction for a unit time (Δt) can be expressed by assuming that the pore water pressure is constant over a small elementary volume of space. This relationship is expressed in Eq. (8):

$$\begin{aligned} Q_x &= \left(\frac{\partial v_x}{\partial x}\mathrm{d}x\right)\mathrm{d}y\mathrm{d}z\mathrm{d}t = \frac{\partial}{\partial x}\left(k_x\frac{\partial h}{\partial x}\right)\mathrm{d}y\mathrm{d}z\mathrm{d}t = k_x \cdot i_x \cdot \mathrm{d}y \cdot \mathrm{d}z \cdot \mathrm{d}t \\ &= k_x \cdot \sin\beta \cdot \mathrm{d}y \cdot \mathrm{d}z \cdot \mathrm{d}t = k_x \cdot \sin\beta \cdot s \cdot H_\mathrm{w} \cdot \mathrm{d}t \end{aligned} \tag{8}$$

where $\sin\beta (= i = \mathrm{d}h/\mathrm{d}s)$ is the hydraulic gradient resulting from a difference in the groundwater potential across an element of the medium. To apply the raster model, the total volume of flow leaving the element (Q_x) in a cell can convert to the change in height (ΔH) using the deficit water content ($\Delta\theta$), and be expressed by

$$\Delta H = \frac{Q_x}{\mathrm{d}x\mathrm{d}y} \cdot \frac{1}{\Delta\theta} = \frac{Q_x}{s^2} \cdot \frac{1}{\Delta\theta} = \frac{k_x \cdot \sin\beta \cdot H_\mathrm{w}}{s \cdot \Delta\theta}\mathrm{d}t \tag{9}$$

where s is the distance between each cell (or size of a cell, $= \mathrm{d}x = \mathrm{d}y$), H_w is the height of groundwater in a cell ($= \mathrm{d}z$), and θ_s is the volumetric water content.

The total volume of flow leaving the element and its flow direction were estimated using the eight-flow method (Jenson and Domingue, 1988). The flow of groundwater was calculated using the slope and slope direction of the bedrock. Based on the assumption that the kinetic energy is negligible, the total volume of flow leaving a cell can only be affected by the neighbourhood cells. It noted that a vector analysis including the watershed and drainage network is not required. Therefore, the flow of groundwater can be calculated from a cell to a neighbourhood by shifting the change of groundwater

NHESSD
2, 5575–5601, 2014

height based on Eq. (9). The variations in the groundwater level in each cell over time are expressed as following Eqs. (10) and (11):

$$\Delta H_{ijk} = \frac{k_s \cdot \sin\beta_{ij} \cdot H_{ijk}}{s \cdot \Delta\theta} \cdot \mathrm{d}t \tag{10}$$

$$\begin{aligned}
&k = t, (\text{initial } H_{ijt} - H_{ij(t-1)})\\
&i = 2, j = 2, H_{22t} = H_{22t} - \Delta H_{22t}\\
&D = 1, H_{23t} = H_{23t} + \Delta H_{22t} : D = 2, H_{33t} = H_{33t} + \Delta H_{22t}\\
&D = 4, H_{32t} = H_{32t} + \Delta H_{22t} : D = 8, H_{31t} = H_{31t} + \Delta H_{22t}\\
&D = 16, H_{21t} = H_{21t} + \Delta H_{22t} : D = 32, H_{11t} = H_{11t} + \Delta H_{22t}\\
&D = 64, H_{12t} = H_{12t} + \Delta H_{22t} : D = 128, H_{13t} = H_{13t} + \Delta H_{22t}
\end{aligned} \tag{11}$$

As mentioned above, the rainfall infiltration was completely recharged into the groundwater with the hydrometeorological model and calculated with Eq. (2). Equation (2) can be represented by Eq. (12) because of the recharge depth, which considers the storage time. Figure 6 shows the flow chart for groundwater flow, which considers the storage time in the YS-Slope.

$$\begin{aligned}
&k = t,\\
&\text{initial } H_{ijt} = H_{ij(t-1)} + I_{R,ij(t-t_s)}\\
&t_s = (H - H_{ijt}) \times K_s\\
&H_{ijt} = H_{ij(t-1)} - \Delta H_{ijt}
\end{aligned} \tag{12}$$

5.5 Summary of the proposed methodology

We propose a conceptual methodology (Fig. 7) for the typical susceptibility assessment of shallow landslide based on hydro-geotechnical method. A computer program, YS-Slope has been developed using this methodology. The YS-Slope uses unsaturated soil parameters such as field matric suction and SWCC. Various types of rainfall events

NHESSD
2, 5575–5601, 2014

like real-time rainfall and probability rainfall are used. They were built to raster data of matrix structure. Using these data and DEM, the rainfall infiltration depth and recharge into the groundwater considering storage time were calculated for different times and locations of watershed. It was used for calculating factor of safety in second level. Finally, it can assess a rainfall-induced landslide depending on time varying by using groundwater table and wetting band depth. The case studies at the Raemian watershed and Dukwooam watershed described in this paper were conducted using this program.

6 Results and discussion

A GIS-based landslide analysis was performed to find out caus[illegible] and failure mechanism by using the YS-Slope model. A 5 m × 5 m gridded DEM converted from the 2009 LiDAR data, soil data obtained from detailed investigations and field measurements, and precipitation gauged by the auto weather station (AWS) of KMA (KMA, 2011) were used as the input data. Landslide inventory was acquired from comprehensive investigation such as a field observation and an aerial light detection and ranging (LiDAR) surveying. The soil inves[illegible]ation was performed to obtain the detailed information of soil properties. The soil properties were est[illegible]ted and are summarised in Table 3, some soil properties were adopted from the literature (Clausnitzer et al., 1998; Norris, 2008; Smit, 2000). The soil layer depth is one of the important parameter in verifying the cause of a disaster. To obtain the soil layer thickness at the study area, a krigging method was performed by using data from 14 boreholes, seismic prospecting, and a DEM.

Figure 8a and b shows the result of the landslide analysis using the proposed model for the test site 1, and the landslides locations investigated in field are marked by black dots. The landslides and debris flows led to erode approximately 67 % of the watershed. The area of erosion from these results was compared with a map of safety factors obtained by using the proposed model, and the result overlapped in the erosion map of Fig. 8a. The proposed model has a limitation to predict landslides in approximately

NHESSD
2, 5575–5601, 2014

49.7 % of the area. The area of 49.7 % is associated with debris flows. Initial material volume triggered by landslide flowed down the valley, and eroded subsurface of these area. Nevertheless, all 6 landslide observations are located within the resultant unstable area by the proposed model. Figure 8b shows the result of rainfall-induced landslide as the types of failure. At the point of L3, L4 and L6 in the landslide inventory, it was assessed that the landslides were occurred under the groundwater, and L1, L2 and L5 on wetting front. Thus, two types of landslide were occurred in this study area, and the series of landslide were triggered by subsurface infiltration and rising groundwater-table.

Figure 8c and d shows the result of the analysis using the predictive models for the test site 2. In this test site, the results of analysis for the both mechanisms reasonably agree with all of landslide observations. Because this site has generally a shallow soil depth of 2.0–3.0 m, it is sufficiently shallow with relation to wetting band depth of 2.0 m in the test site. Thus, this area was exposed to the same level of risk of landslide, which was triggered by subsurface infiltration and rising groundwater-table. The results show the primary triggering factors causing landslides, i.e. soil depth, and spatial and temporal distributions of groundwater variations. It is shown that the YS-Slope model which takes into these factors account can be an intermediate approach between the detailed and simple analytical methods.

7 Conclusions

The primary object of this study was to investigate a landslide on Umyeonsan (Mt.) and to develop the conceptual methodology of landslide design. A comprehensive study was carried out on the cause and mechanism of landslide. The proposed model was used to assess the susceptibility of landslide for two study areas. The following conclusions can be drawn from the findings of this study:

Instability of soil slopes can be predicted by observing changing matric suction distributions spatially and temporally over the soil slope cross section. We develop

NHESSD
2, 5575–5601, 2014

the conceptual methodology of landslide design based on in-situ tests and numerical analyses which consider the important mechanism of groundwater flow and rainfall-infiltration. It is noted that the proposed model which takes into these factors account can be more suitable than previous models (Baum et al., 2008; Montgomery et al., 1994; Pack et al., 1998; Tarboton et al., 1997) due to its capability to model combing 1-D-infilatriaon process in unsaturation conditions and 2-D-groundwater flow in steady-state conditions. Thus, despite its simplicity, this model is capable of adopting in large scale analysis.

The proposed model has been improved by incorporating the combined effects of groundwater flow and rainfall infiltration into the raster model. These elements were integrated into the infinite slope-stability model for a rainfall-induced landslide. The special attention is given to the consideration of groundwater flow, rainfall water infiltration into ground and groundwater rising in ground. Existing models do not consider the three factors simultaneously.

The proposed model has clearly demonstrated that two types of rainfall induced landslide were covered: in the study area 1, the series of landslide were triggered by rainfall water infiltration into ground and groundwater rising in ground. In the other hand in the study area 2, two types of landslide mechanism had all good agreement with landslide observation. It is indicated that a case of shallow depth of soil like as the study area 2 should be exposed to the same level of risk of landslide, which was triggered by subsurface infiltration and rising groundwater-table.

Acknowledgements. This work was supported by the National Research Foundation of Korea (NRF) grant funded by the Korea government (MSIP) (No. 2011-0030040).

NHESSD
2, 5575–5601, 2014

References

ASTM: Annual Book of ASTM Standards: Measurement of Soil Potential (Suction) Using Filter Paper, Vol. 04.08, ASTM, 154–159, 2000.

Baum, R. L., Savage, W. Z., and Godt, J. W.: TRIGRS – a Fortran Program for Transient Rainfall Infiltration and Grid-Based Regional Slope-Stability Analysis, Version 2.0, US Geological Survey, 2008.

Cedergren, H. R.: Seepage, Drainage and Flow Nets, 2nd Edn., Wiley, New York, 1977.

Clausnitzer, V., Hopmans, J., and Starr, J.: Parameter uncertainty analysis of common infiltration models, Soil Sci. Soc. Am. J., 62, 1477–1487, 1998.

Fredlund Gray, D. H.: Biotechnical and Soil Bioengineering Slope Stabilization: a Practical Guide for Erosion Control, Wiley, New York, 1978.

Green, W. H. and Ampt, G.: Studies on soil physics, 1. The flow of air and water through soils, J. Agr. Sci., 4, 1–24, 1911.

Hammond, C., Hall, D., Miller, S., and Swetik, P.: Level I Stability Analysis (LISA) Documentation for Version 2.0, US Department of Agriculture, Forest Service, Intermountain Research Station, 1992.

IPCC – Intergovernmental Panel on Climate Change: Climate Change 2007, The Physical Science Basis: Working Group I Contribution to the Fourth Assessment Report of the IPCC, Fourth Assessment Report, Cambridge university press, Cambridge, UK and New York, NY, USA, 2007.

Jenson, S. and Domingue, J.: Extracting topographic structure from digital elevation data for geographic information system analysis, Photogramm. Eng. Rem. S., 54, 1593–1600, 1988.

Jeong, S., Kim, J., and Lee, K.: Effect of clay content on well-graded sands due to infiltration, Eng. Geol., 102, 74–81, 2008.

Kim, J., Jeong, S., Park, S., and Sharma, J.: Influence of rainfall-induced wetting on the stability of slopes in weathered soils, Eng. Geol., 75, 251–262, 2004.

Kim, J., Jeong, S., and Regueiro, R. A.: Instability of partially saturated soil slopes due to alteration of rainfall pattern, Eng. Geol., in press, 2012.

KMA – Korean Meteorological Administration: Weather Information, available at: http://kma.go.kr/weather/observation/aws_table_popup.jsp, 2011.

Mein, R. G. and Larson, C. L.: Modeling infiltration during a steady rain, Water Resour. Res., 9, 384–394, 1973.

NHESSD
2, 5575–5601, 2014

Montgomery, D. R. and Dietrich, W. E.: A physically based model for the topographic control on shallow landsliding, Water Resour. Res., 30, 1153–1171, 1994.
Norris, J. E.: Slope Stability and Erosion Control: Ecotechnological Solutions, Springer, Dordrecht, the Netherlands, 2008.
Pack, R., Tarboton, D., and Goodwin, C.: The SINMAP Approach to Terrain Stability Mapping, 8th Congress of the International Association of Engineering Geology, Vancouver, British Columbia, Canada, 21–25, 1998.
Pham, H. Q. and Fredlund, D. G.: New Apparatus for the Measurement of the Soil-Water Characteristic Curves, Proceedings of the 57th Canadian Geotechnical Conference, Quebec, Quebec City, Canada, 2004.
Pradel, D. and Raad, G.: Effect of permeability on surficial stability of homogeneous slopes, J. Geotech. Eng., 119, 315–332, 1993.
Smit, A. L.: Root Methods: a Handbook, Springer, Heidelberg, Germany, 2000.
Soller, D. R. and Berg, T. M.: The US national geologic map database project: overview & progress, in: The Current Role of Geological Mapping in Geosciences, Springer, 245–277, 1999.
Soller, D. R., Duncan, I., Ellis, G., Giglierano, J., and Hess, R.: Proposed Guidelines for Inclusion of Digital Map Products in the National Geologic Map Database, Digital Mapping Techniques'99 – Workshop Proceedings, US Geological Survey Open-File Report, UA Geological Survey, Dordrecht, the Netherlands, 99–386, 2005.
Tarboton, D. G.: A new method for the determination of flow directions and upslope areas in grid digital elevation models, Water Resour. Res., 33, 309–319, 1997.
Vanapalli, S., Fredlund, D., Pufahl, D., and Clifton, A.: Model for the prediction of shear strength with respect to soil suction, Can. Geotech. J., 33, 379–392, 1998.
Van Genuchten, M. T.: A closed-form equation for predicting the hydraulic conductivity of unsaturated soils, Soil Sci. Soc. Am. J., 44, 892–898, 1980.

NHESSD
2, 5575–5601, 2014

Table 1. Estimated coefficient of the van Genuchten model (Van Genuchten, 1980).

Curve-fitting parameters	Value
$\alpha(1/\text{kPa})$	11.3
N	1.35
$m = 1 - 1/n$	0.25
Saturated volumetric water content (θ_s)	0.5
Residual volumetric water content (θ_r)	0.18

NHESSD
2, 5575–5601, 2014

Table 2. The procedure to determine the recharge depth over time.

Step	Procedure
1	Calculation of wetting band depth (①) using $\Delta\theta(\theta_s - \theta_{i,0}$ or $\theta_s - \theta_{i,1})$.
2	Changing (①) to depth of the unsaturated zone (②) using $\Delta\theta(\theta_{i,1} - \theta_{i,0})$ until (②) is not exceed soil depth .
3	Calculation of recharge depth using $\Delta\theta(\theta_s - \theta_{i,1})$ when (②) is larger than H.
4	Calculation of groundwater flow.
5	Repeat process of (1)–(4) in each cells

NHESSD
2, 5575–5601, 2014

Table 3. Geotechnical and hydraulic properties of the soil used in this study.

Parameters	Values
Hydraulic conductivity, k_s	8×10^{-4} cm s^{-1} (28.8 mm h^{-1})
Initial water contents, θ_i	28.0–32.0 (30.0) %
Water-content deficit, $\Delta\theta$	0.20
Wetting front suction head, ψ_f	830 mm
Soil cohesion, C'_s	10.2–12.8 (11.0) kPa
Soil friction angle, ϕ'	22.4–26.6 (26.5) degree
Total unit weight of soil, γ_t	17.0–18.5 (18.0) kN m^{-3}
Additional shear strength by roots of tree, C'_r	1.0 kPa
Uniform load from tree, q_0	0.253 kPa

Parenthesis indicates number of average.

NHESSD
2, 5575–5601, 2014

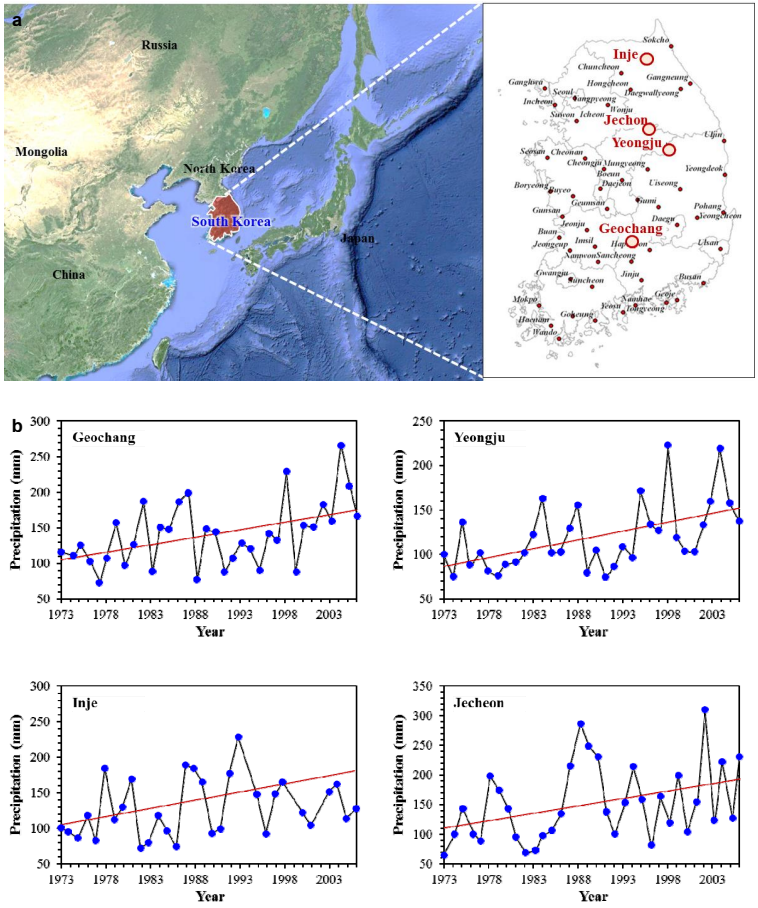

Figure 1. Rainfall records and climate change in South Korea. **(a)** 56 weather stations in South Korea (Kim et al., 2010), **(b)** annual daily maximum rainfall at 4 weather stations in South Korea.

NHESSD
2, 5575–5601, 2014

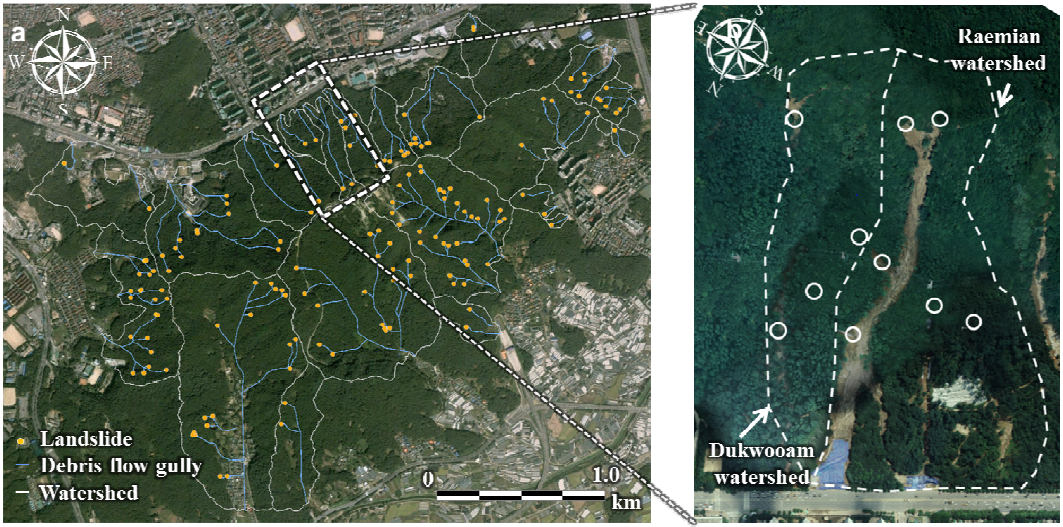

Figure 2. Landslides triggered in the Umyeonsan (Mt.) under heavy rainfall (307 mm day^{-1}) in 2011 on Mountain landslides in 2011. **(a)** Location map of landslides in 2011, **(b)** general view of the landslides in study areas; Raemian watershed and Dukwooam watershed.

NHESSD
2, 5575–5601, 2014

Susceptibility assessment of landslides under extreme-rainfall events

S. S. Jeong et al.

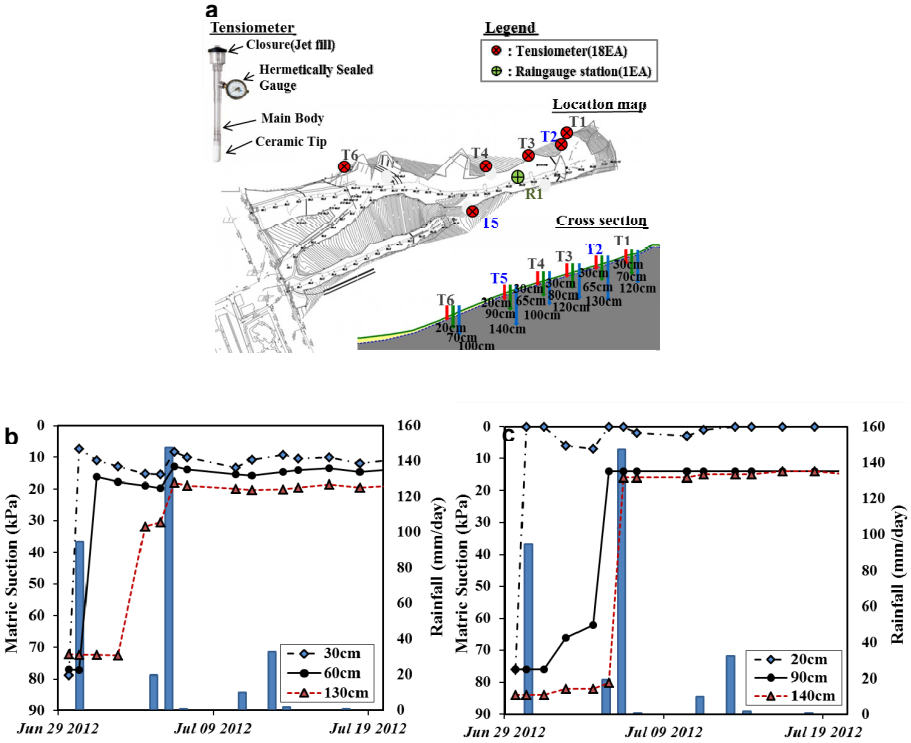

Figure 3. Field instrumentation and measurement for a change of matric suction response to rainfall. **(a)** Location map, cross section and instrument of field measurement, **(b)** typical measurement results and rainfall data: T2 (−30, −60, −130), c: T5 (−20, −90, −140).

NHESSD
2, 5575–5601, 2014

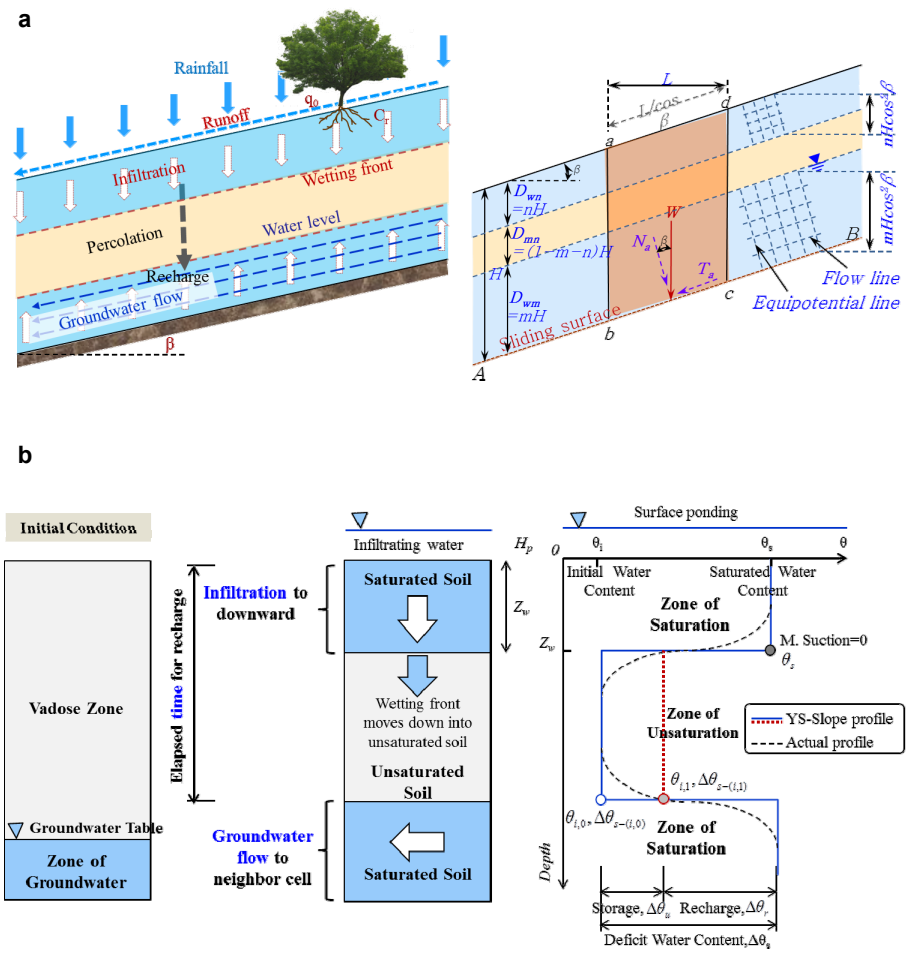

Figure 4. Schematic diagram of the YS-Slope model. **(a)** Infinite slippage plane for slope stability analysis, **(b)** soil profile and hydrologic model concept.

NHESSD
2, 5575–5601, 2014

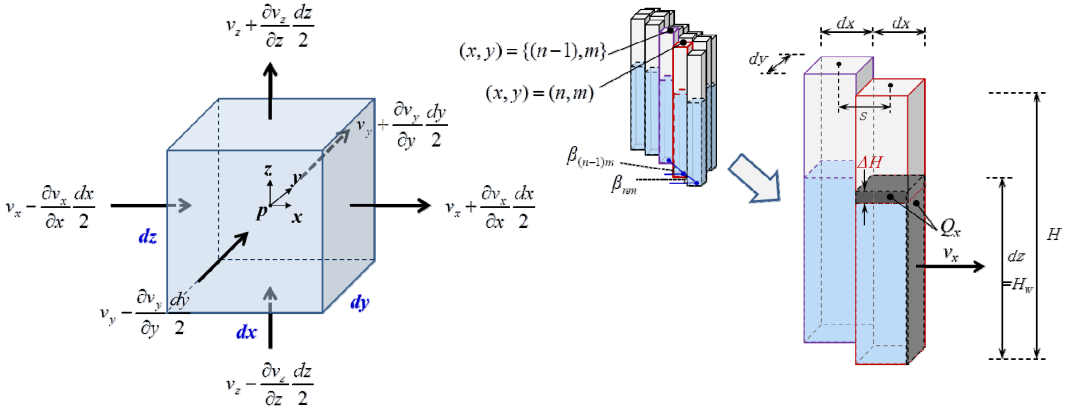

Figure 5. Fluid flow of an elementary volume of fluid in YS-slope.

NHESSD
2, 5575–5601, 2014

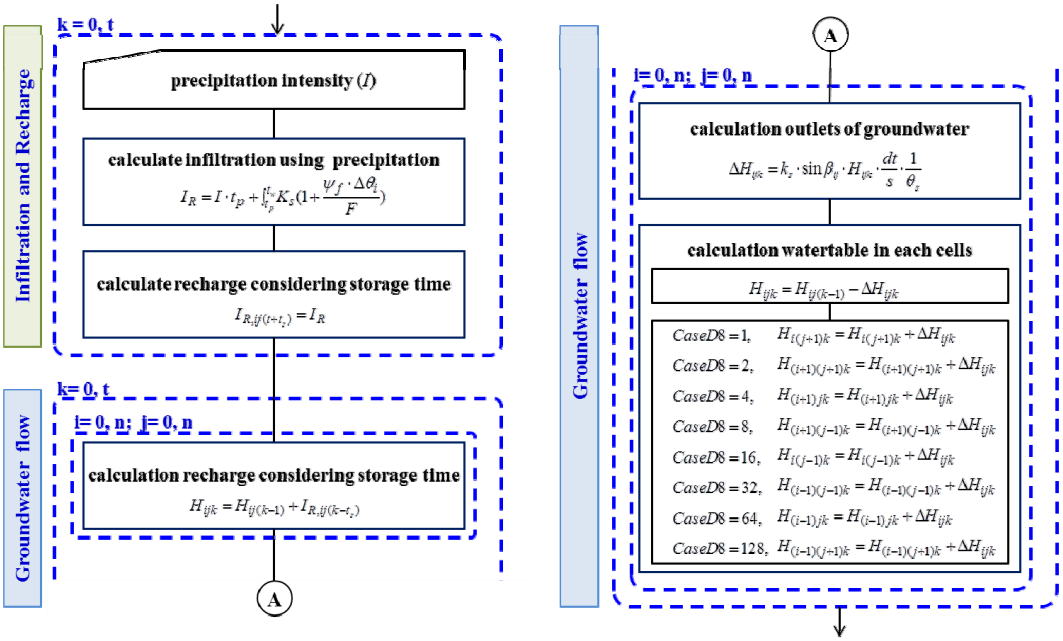

Figure 6. Flow chart of groundwater flow calculation in the YS-slope.

NHESSD
2, 5575–5601, 2014

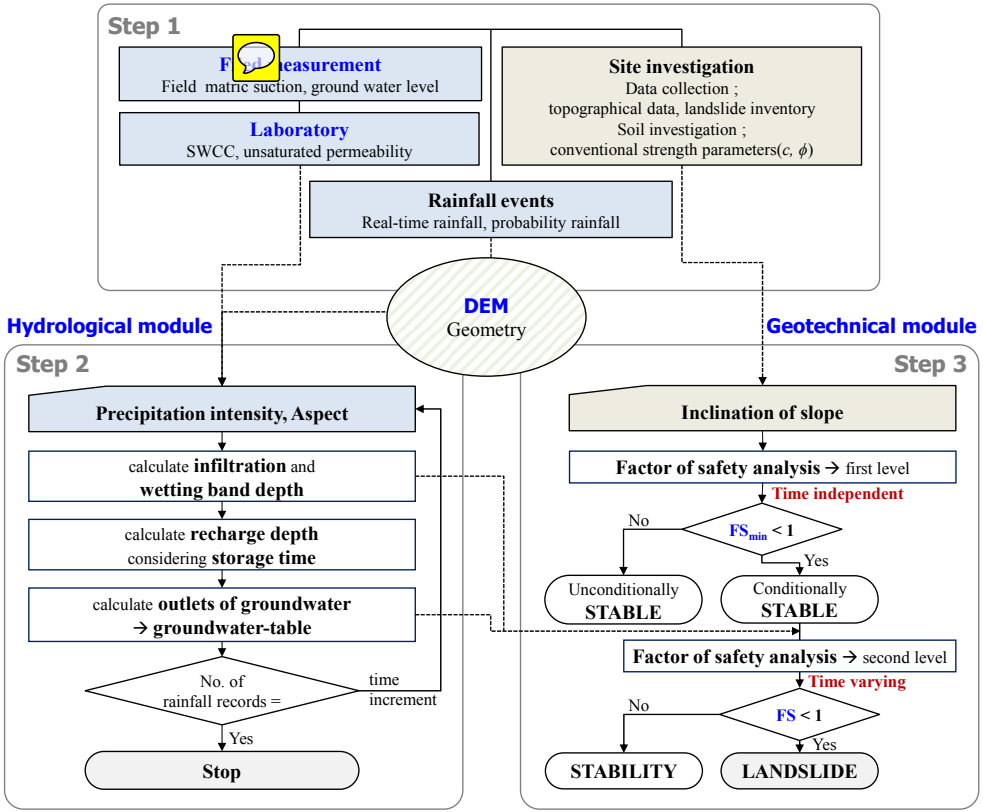

Figure 7. Flow chart of the proposed conceptual methodology.

NHESSD
2, 5575–5601, 2014

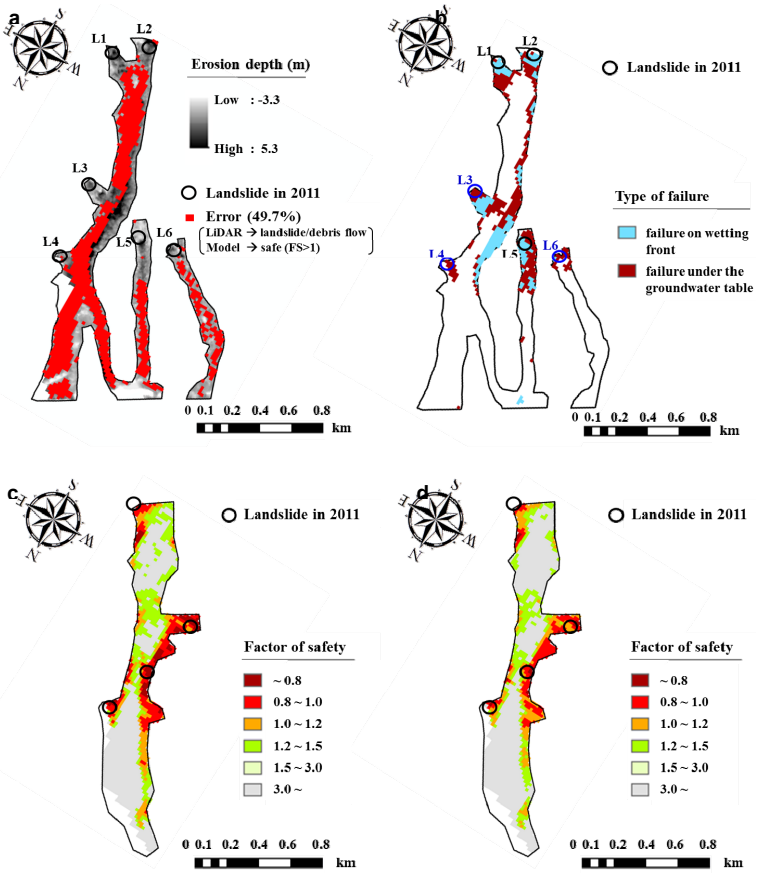

Figure 8. Landslide case on the Raemian and Dukwooam watersheds in 2011. **(a)** Comparison between erosion depth from LiDARs and stability by using physically-based model (test site 1), **(b)** type of slope failure (test site 1), **(c)** slope failure under the groundwater table (test site 2), **(d)** failure on wetting front (test site 2).

NHESSD
2, 5575–5601, 2014